Geological Society, London, Special Publications

Subducting slab structure below the eastern Sunda arc inferred from non-linear seismic tomographic imaging

S. Widiyantoro, J. D. Pesicek and C. H. Thurber

Geological Society, London, Special Publications 2011, v.355; p139-155.
doi: 10.1144/SP355.7

Notes

Subducting slab structure below the eastern Sunda arc inferred from non-linear seismic tomographic imaging

S. WIDIYANTORO[1]*, J. D. PESICEK[2] & C. H. THURBER[2]

[1]*Faculty of Mining and Petroleum Engineering, Bandung Institute of Technology, Jl. Ganesha 10, Bandung 40132, Indonesia*

[2]*Department of Geoscience, University of Wisconsin-Madison, 1215 W Dayton St., Madison WI 53706, USA*

**Corresponding author (e-mail: sriwid@geoph.itb.ac.id)*

Abstract: Detailed P-wave speed velocity structure beneath the Sunda arc has been successfully imaged by applying a non-linear approach to seismic tomography. Nearly one million compressional phases from events within the Indonesian region have been used. These include the surface-reflected depth phases pP and pwP in order to improve the sampling of the upper-mantle structure, particularly below the back-arc regions. We have combined a high-resolution regional inversion with a low-resolution global inversion to minimize the mapping of distant aspherical mantle structure into the study region. In this paper, we focus our discussion on the upper mantle structure beneath the eastern part of the Sunda arc. The tomographic images confirm previous observations of a hole in the subducted slab in the upper mantle beneath eastern Java. The images also suggest that a tear in the slab exists below the easternmost part of the Sunda arc, where the down-going slab is deflected in the mantle transition zone. In good agreement with previous studies, the properties of the deflected slab show a strong bulk-sound signature.

The Sunda arc, located in the western part of the Indonesian region, extends from northwestern Sumatra to Flores, that is, to the west of the Banda arc-Australian continent collision zone. The Sunda arc marks the subduction of the Indo-Australian plate beneath the Eurasian plate. The age of the incoming plate varies laterally. It is relatively young along Sumatra, where subduction is highly oblique. In contrast, below the eastern part of the Sunda arc (i.e. Java and small islands east of it), the age of the subducted plate is significantly older and the convergence direction is almost perpendicular to the arc. Mueller *et al.* (1997) suggest that the age of the incoming oceanic plate ranges from 40 Ma beneath northern Sumatra to 110 Ma south of Java. The lateral variation of the nature and age of the incoming plate influences the style of deformation and seismicity along the Sunda arc (Cloetingh & Wortel 1986). The character of subduction-related seismicity changes abruptly from Sumatra to Java. Seismicity does not exceed a depth of 300 km beneath Sumatra, except for some small events in the southeastern part of the island, but earthquakes occur at depths of up to *c*. 670 km below Java to the east (Fig. 1).

The convergence rate of the Indo-Australian and Eurasian plates in general increases from Sumatra to the easternmost part of the Sunda arc (Minster & Jordan 1978). Tregoning *et al.* (1994) measured convergence rates of 6.7 ± 0.7 cm a^{-1} across the Java trench between Christmas Island, SW of Java, and west Java in a direction of N11°E $\pm$ 4°. This is similar to the relative plate velocity between Australia and Eurasia predicted by the NUVEL-1A plate motion model (DeMets *et al.* 1994). The movement of Australia northward caused rotation of blocks and accretion of microcontinental fragments to SE Asia (Hall 2002). With this complex tectonic setting, it can be expected that the Sunda arc overlies a heterogeneous mantle partly evident from its seismicity (Fig. 1).

Previous seismic tomographic studies of mantle structure below the study region focused on the deep subduction of the Indo-Australian plate. The imaged slab penetrates directly into the lower mantle, where it deflects in the uppermost lower mantle and sinks almost vertically to a depth of at least 1200 km (Fukao *et al.* 1992; Puspito *et al.* 1993; Widiyantoro & van der Hilst 1996, 1997; Bijwaard *et al.* 1998). The aim of this study is to explore the detailed structure of slabs in particular in the upper mantle beneath the eastern Sunda arc, where a pronounced seismic gap exists in a depth interval of *c*. 250–450 km (e.g. Newcomb & McCann 1987) and a hole in the subducted slab has been reported (Hall *et al.* 2009). We present new P-wave seismic images produced by means of an improved tomographic imaging technique (Pesicek

From: HALL, R., COTTAM, M. A. & WILSON, M. E. J. (eds) *The SE Asian Gateway: History and Tectonics of the Australia–Asia Collision*. Geological Society, London, Special Publications, **355**, 139–155.
DOI: 10.1144/SP355.7 0305-8719/11/$15.00

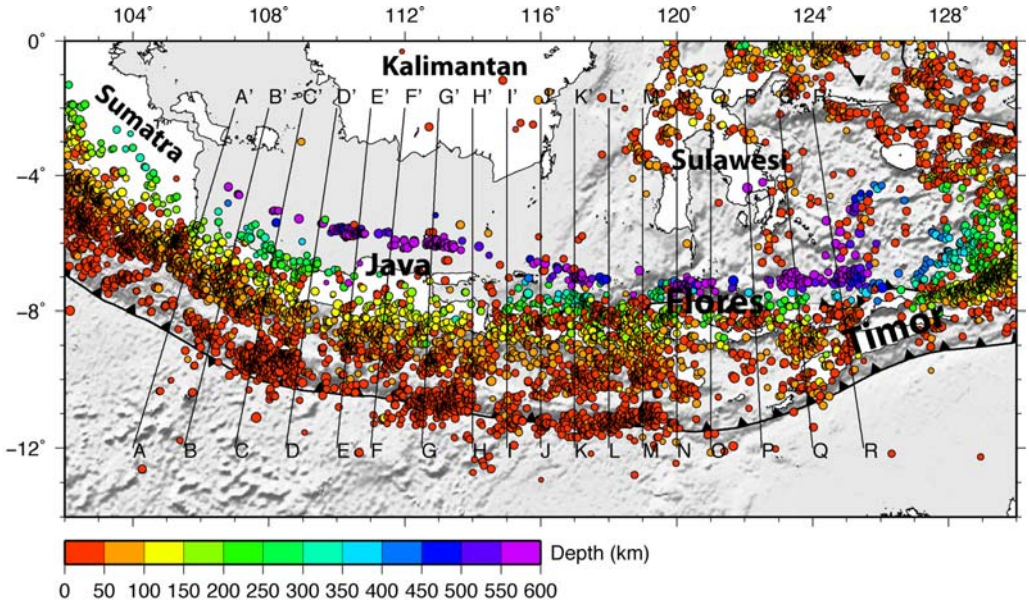

Fig. 1. Map of the study region. Circles depict the epicentres of relocated events (Engdahl *et al.* 1998, 2007) in the region occurring between 1964 and 2007, with colours denoting the hypocentre depths. Black lines indicate the position of the vertical cross sections displayed in Figures 4 and 8.

et al. 2010). We note that P-wave tomographic images of the subduction zone west of the present study area (i.e. below the western Sunda arc) have been presented in detail by Pesicek *et al.* (2008, 2010). Herein we discuss only the eastern Sunda arc and present new S-wave images to enhance our discussion and interpretations.

Data and method

Data

Engdahl *et al.* (1998) carefully relocated nearly 100 000 earthquakes that occurred between 1964 and 1995 by using a nonlinear scheme and the radially stratified ak135 velocity model developed by Kennett *et al.* (1995). These data consist of *c*. 13 million P, pP, pwP, PKP and S phase arrival times reported by almost 6000 globally distributed seismographic stations. In this study, we have used an updated data set covering the period 1964 to 2007 (Fig. 1). In the western Sunda arc region, the new data set has been further groomed to provide more accurate depths (Engdahl *et al.* 2007). The updated dataset consists of 957 262 compressional phases from events within the Indonesia region, including 10 640 pP and 4239 pwP phases. Detailed data selection criteria are presented in Pesicek *et al.* (2010).

Method

We have used a cellular representation of mantle structure by discretizing the entire mantle using cells of $5^\circ \times 5^\circ$ (with 16 layers down to the bottom of the mantle), but in the study region we have employed a finer grid of $0.5^\circ \times 0.5^\circ$ (with 19 layers down to 1600 km) in order to allow the resolution of relatively small-scale structures. Such a model parameterization minimizes contamination by structures outside the volume being investigated (Fukao *et al.* 1992; Widiyantoro & van der Hilst 1996, 1997). We solved for perturbations to 178 272 model slowness cells using the iterative LSQR algorithm (Paige & Saunders 1982), a conjugate gradient technique first used in seismic tomography by Nolet (1987); see also Spakman & Nolet (1988). Following Bijwaard & Spakman (2000) and Widiyantoro *et al.* (2000), we used a step-wise procedure to solve the non-linear travel-time inversion for seismic velocity variations. In the main step, ray paths and travel times are updated by 3D ray tracing through intermediate realizations of the model. The 3D ray tracing is based on the pseudo-bending method of Koketsu & Sekine (1998), originally developed by Um & Thurber (1987). In this study, this procedure was improved upon by use of an *a priori* global crustal model (CRUST 2.0; Bassin *et al.* 2000) in order to reduce the initial residual variance of the data (Pesicek *et al.* 2010).

In the Indonesian region, we initially traced rays from stations to sources through the global spherically symmetric model ak135 (Kennett *et al.* 1995). We then replaced the shallowest layer with velocity values from the *a priori* crustal model. We remark that the images produced by this nonlinear inversion are comparable to those of a one-step linearization (Pesicek *et al.* 2008), but the progressive updating of the slowness field and ray paths results in larger magnitudes of the wave speed perturbations of *c*. 30%.

Presentation of seismic tomograms

We interpret P-wave travel-time residuals in terms of velocity perturbations relative to the ak135 reference velocity model (Kennett *et al.* 1995). In this section we present the images achieved after conducting five iterations with sources fixed to update the 3D velocity model (Pesicek *et al.* 2010).

In Figure 2, we present P-wave velocity anomaly maps for depths representing the upper mantle and transition zone. From the tomographic inversions, we infer that the subducted slab is defined by a laterally continuous region of higher-than-average P-wave velocity in the upper mantle and transition zone. Most parts of the region of interest, in particular along the island arc, are sufficiently sampled by seismic rays and reasonably resolved (Fig. 3). In the upper mantle and transition zone, the dimension of the smallest feature that is resolved is about 100–200 km. Notice that resolution generally degrades with increasing distance away from the slab due to irregular and/or poor sampling. With this and the limitations of the resolution tests in mind we only interpret the large-scale structures.

The image of the slab in the uppermost mantle resembles the present-day Java trench and parallels the present-day Sunda arc. A high velocity slab is detected beneath Java and islands to the east, but hardly seen beneath eastern Java at depths around 250–450 km (Fig. 2). Further examination of anomaly maps for different depth intervals indicates that the fast slab is also absent at shallower depths below the easternmost part of the Sunda arc.

The complexity of the inferred slab structure is further illustrated by vertical sections across the eastern Sunda arc (Fig. 4). The images in Figure 4 suggest that the Indo-Australian plate dips steeply beneath the Java arc and is only partially outlined by a seismic zone. The magenta dashed lines on the cross sections depict our preferred interpretation of the subduction angles. In general, the velocity images and the seismicity reveal a gently dipping slab (10–30°) from the trench to the arc. Then the slab dips more steeply (*c*. 60–70°) down to the transition zone. However, it appears that the dip changes to nearly vertical at depths of about 400 km below the eastern Sunda arc, where the slab is deflected in the transition zone (cross sections O–R in Fig. 4). The seismogenic slab seems to be continuous, except beneath eastern Java (see cross sections E–G in Fig. 4) where a pronounced seismic gap is observed between 250 and 450 km depth. Further east (cross sections K–M in Fig. 4), we detected higher-than-average seismic velocities, but with smaller amplitudes than elsewhere. The amplitude reduction in the seismic gap may suggest a 'necking' of the slab (cf. Widiyantoro & van der Hilst 1996, 1997).

The summary of our observations and interpretations is represented by the 3D smoothed isosurface plot for +0.85% velocity perturbation illustrating the subducted slab in the upper mantle beneath the eastern Sunda arc and the western part of the Banda arc (Figs 5 & 6). Here, the hole in the slab below eastern Java and a tear in the slab beneath the easternmost part of the Sunda arc and perhaps also beneath the Banda arc are clearly depicted, while the small hole below Flores is related to the 'necking' of the slab.

Additionally, we present S-wave tomograms derived by using an updated version of the reprocessed S arrival time data of Engdahl *et al.* (1998). Information from S-wave data helps characterize the inferred velocity variations but previous studies have not produced good constraints on slab structure (e.g. Zhou & Clayton 1990). This is likely due to the relatively high noise level of the International Seismological Centre (ISC) S-wave data. However, refinement of the travel time data, particularly the reprocessing of multiple data sets to extract improved S-wave information conducted by Engdahl *et al.* (1998), has greatly benefited the current study. Engdahl *et al.* (1998) used S phases in the initial source location and an appropriate S-wave reference velocity model (ak135; Kennett *et al.* 1995). Most aspects of the S-wave tomographic imaging technique employed here are similar to those of the P-wave data, except that for a ray to be included in the inversion, the travel-time residual for S relative to the ak135 reference model has to lie in the range ± 15.0 s, in contrast to the dynamic reweighting of P-wave residuals (Pesicek *et al.* 2010).

Figures 7 and 8 contain the resulting S-wave images displayed in the same style as the P-wave images given in Figures 2 and 7 in order to provide direct comparison. Notice that in general the S-wave images depict the slab in the upper mantle well, although some smearing occurs in particular in the uppermost mantle. In the following section we discuss our observations based on the P- and S-wave images and relate them to tectonic processes in the region.

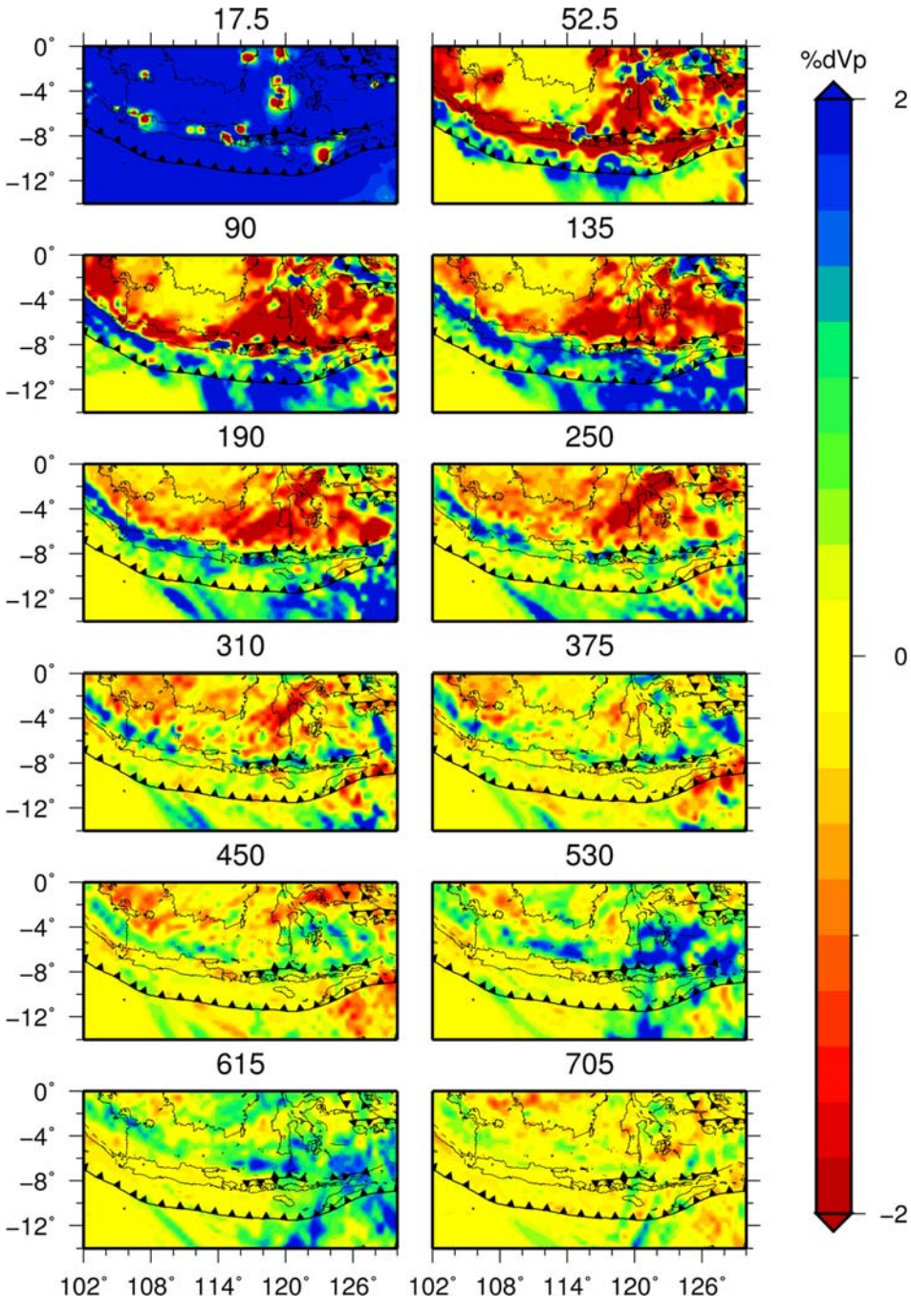

Fig. 2. Layer anomaly maps depicting results of the inversion using full P-wave arrival time data for upper-mantle and transition zone structures below the eastern Sunda arc. Velocity perturbations relative to ak135 developed by Kennett *et al.* (1995) are shown from −2% to +2%. For each map, mid-layer depths are listed in km at the top. The top layer anomaly map has had a crustal correction applied using the global crustal model CRUST 2.0 (Bassin *et al.* 2000) in the study region, as discussed by Pesicek *et al.* (2010). The image of the slab in the upper mantle (from 52.5–450 km) parallels the present-day Sunda trench. Notice the broadening in map view of the slab beneath the easternmost part of the Sunda arc at depths of around 530–615 km.

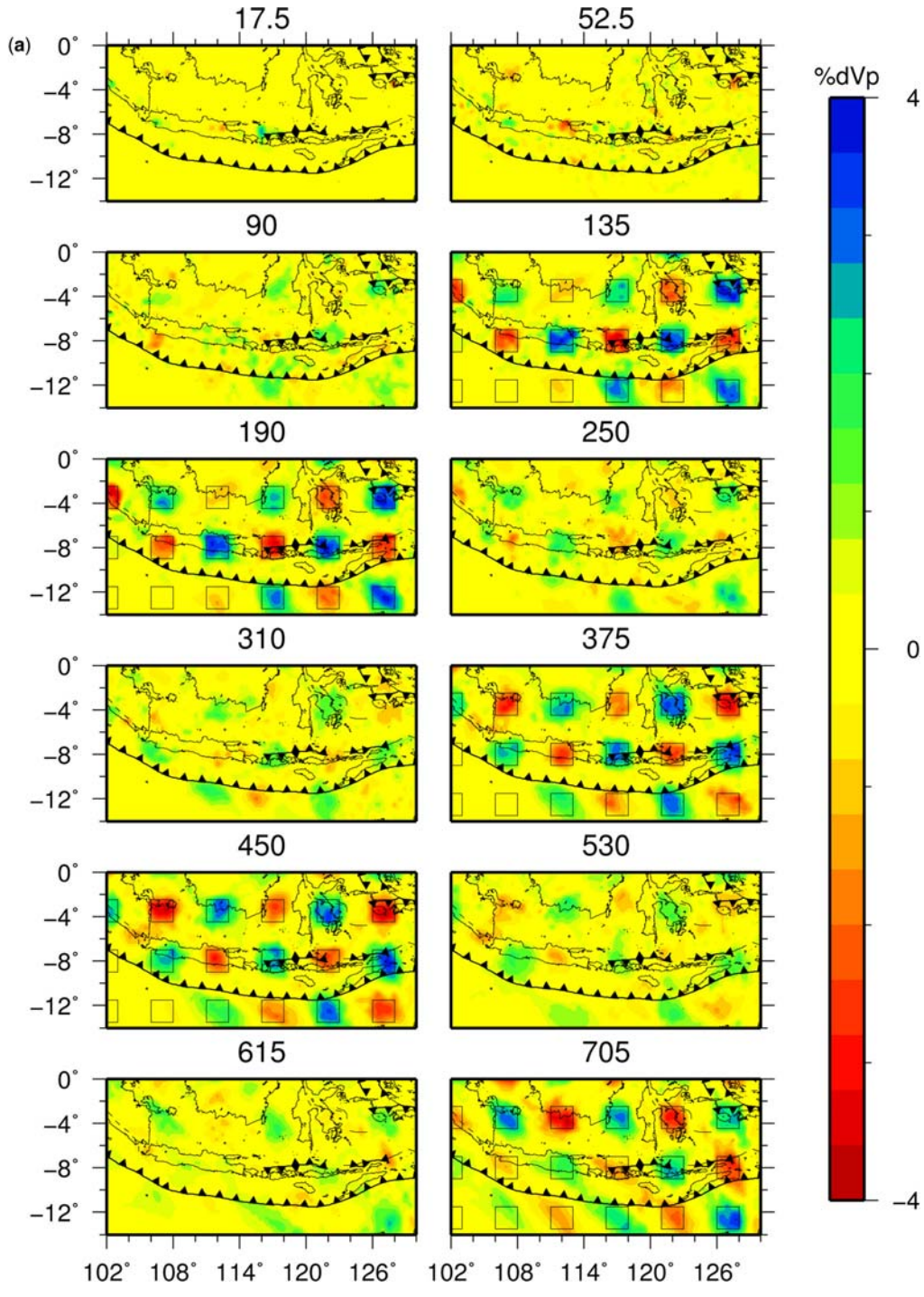

Fig. 3. Resolution tests calculated using the same parameters as the real data inversion. Noise was added based on the actual, but randomized, residual distribution following Pesicek *et al.* (2010). (**a**) Spike model resolution tests after two iterations. Synthetic 4% velocity perturbation input spike anomalies (2.5 × 2.5°; black contours) are separated by 2.5° in latitude and longitude and by 2 layers in depth. Depths with no input anomalies are shown and the perturbations in these layers are an indication of vertical smearing.

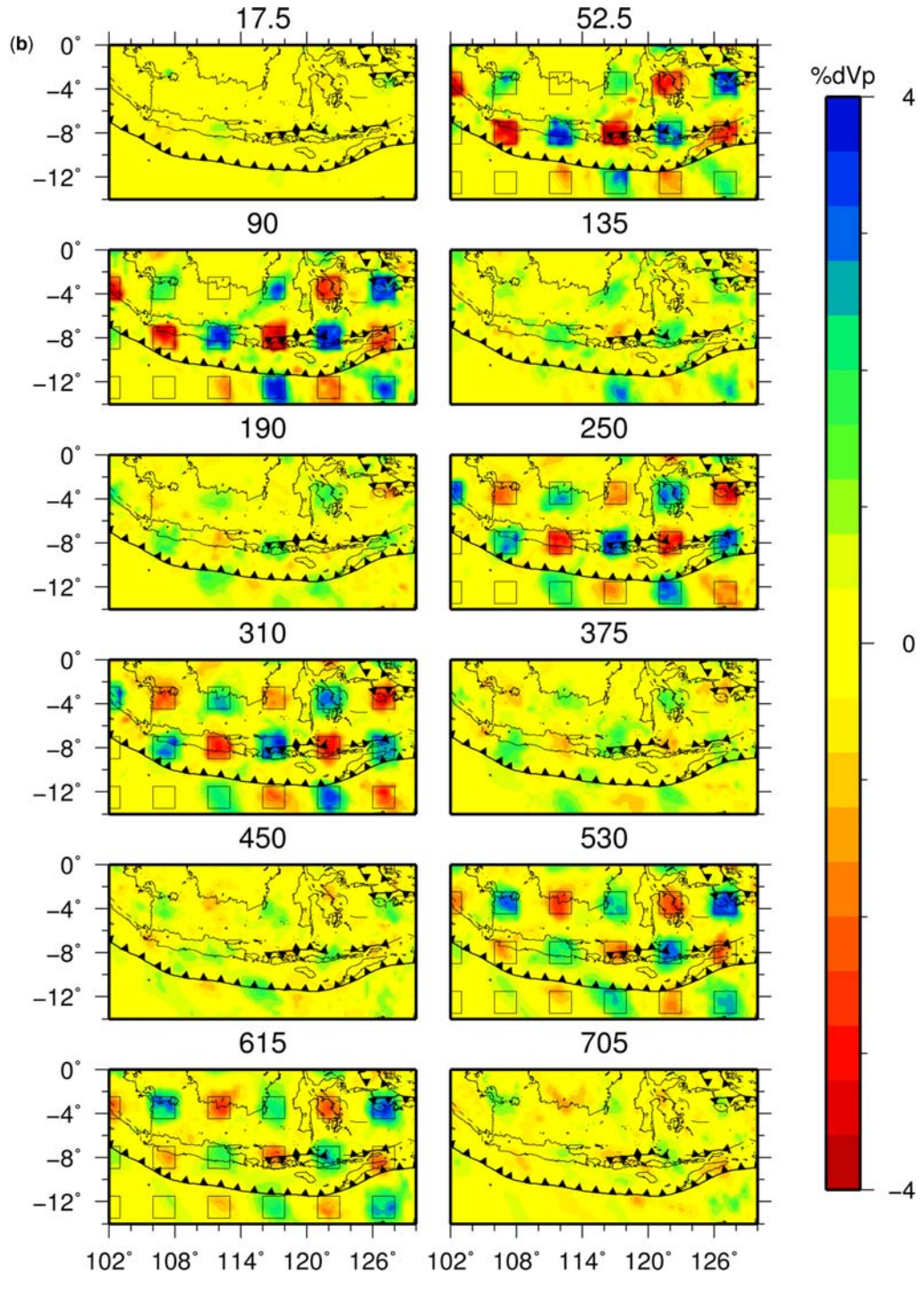

Fig. 3. (*Continued*) (**b**) Alternate spike model, the same as (a) except the input pattern is shifted to be the opposite of (a), that is, layers with (without) anomalies in (a) now lack (have) them.

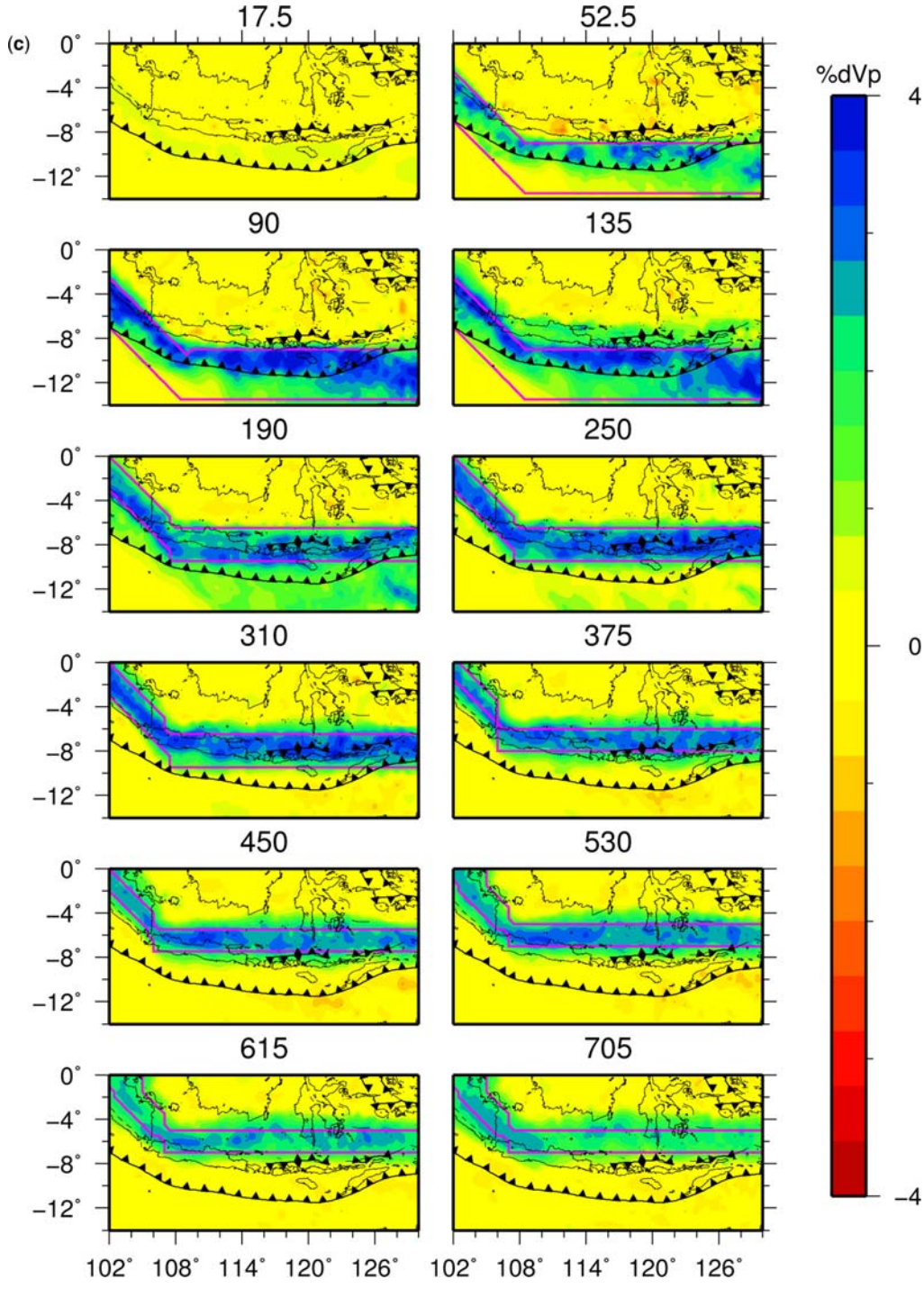

Fig. 3. (*Continued*) (**c**) Synthetic slab resolution test. In general, the synthetic slab (4% velocity perturbation) is well recovered north of the Java trench. The geometry of the synthetic slab is shown by magenta contours in each layer where it is present.

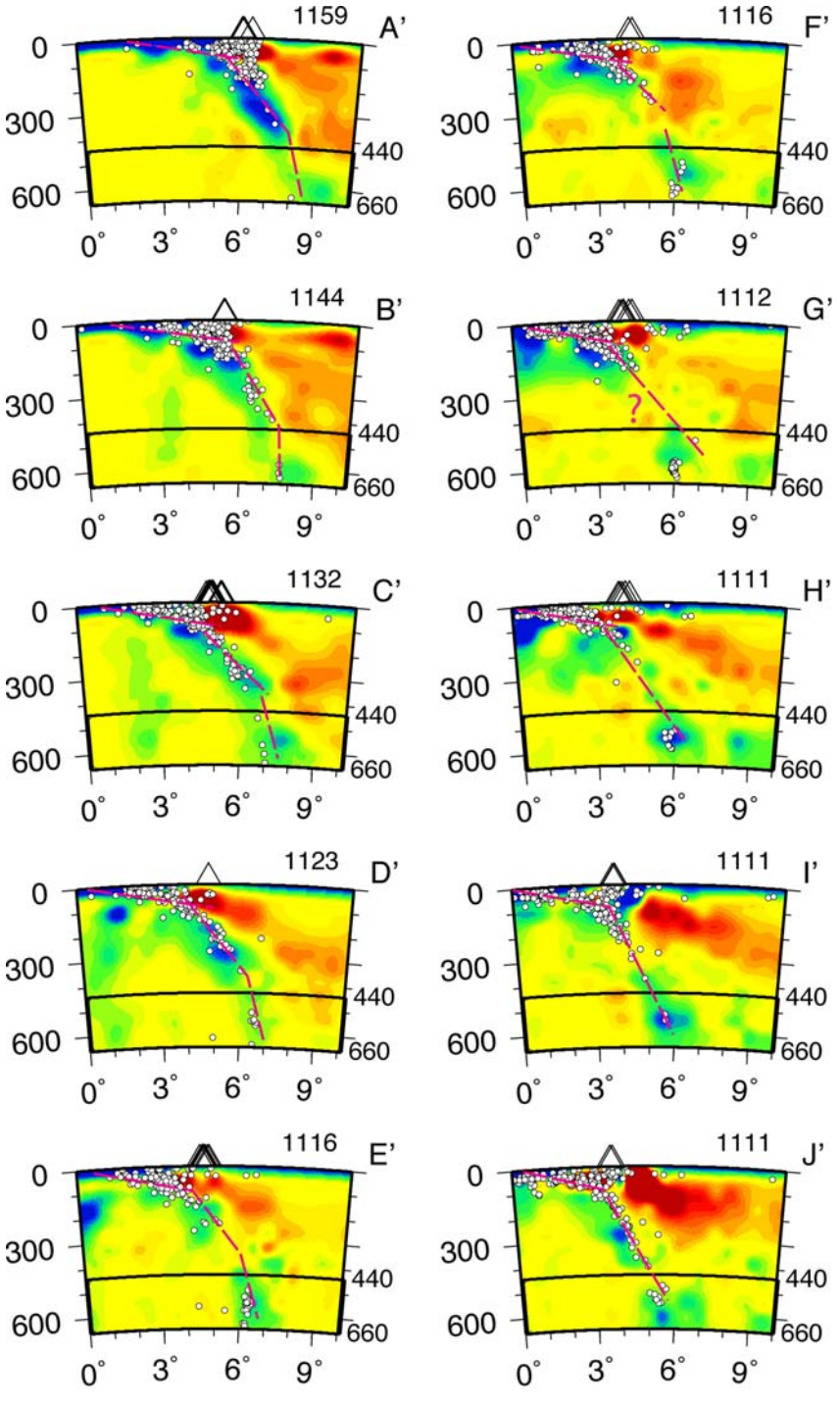

Fig. 4. Vertical sections across the convergent margin in the eastern part of the Sunda arc through the P-wave model plotted as velocity perturbations relative to ak135. Contour scales are from −2% to +2%. Circles depict earthquake hypocentres projected from a distance of up to 55 km on both sides of the plane of section. Magenta dashed lines depict our preferred interpretation of the subduction angle.

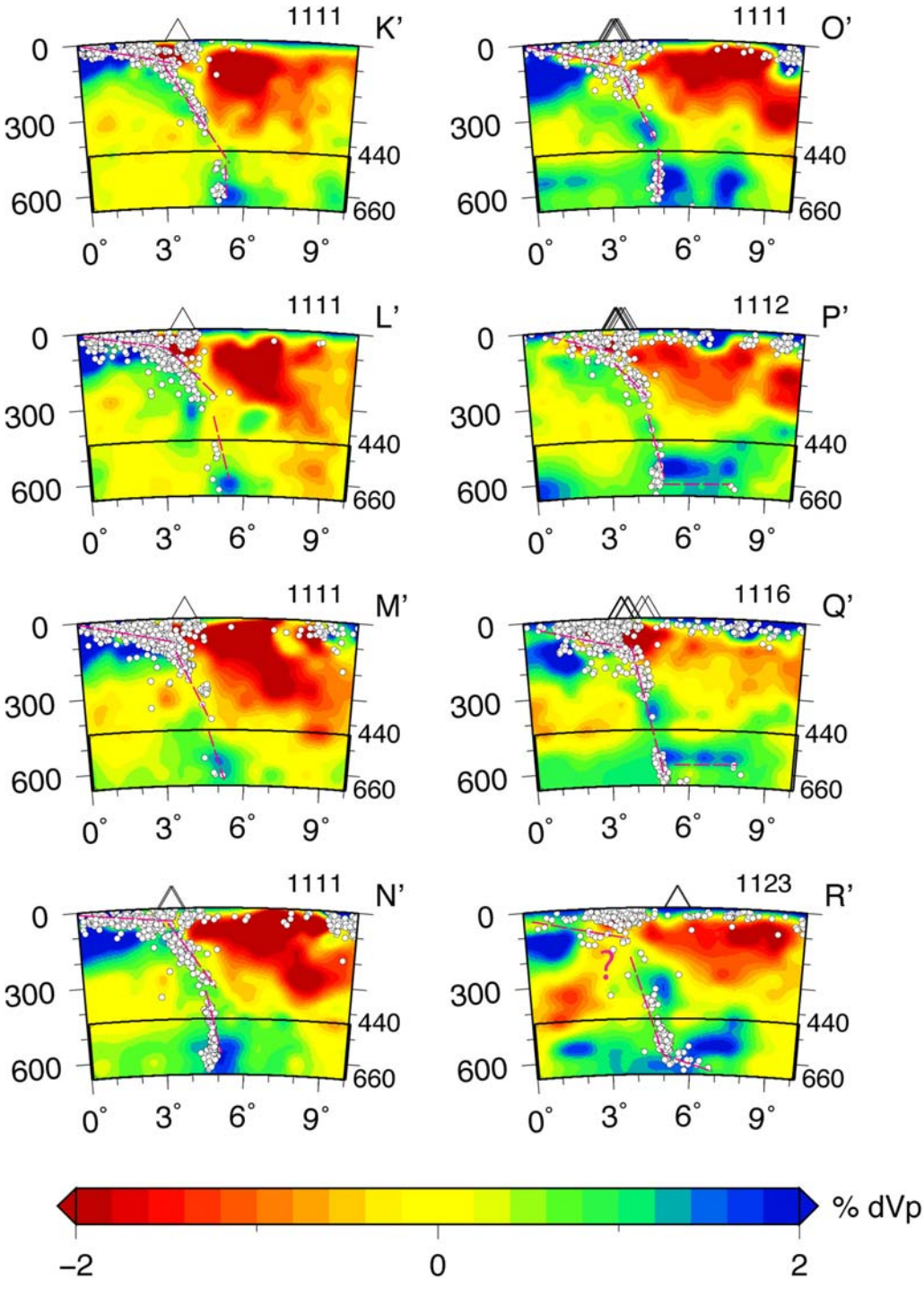

Fig. 4. (*Continued*) For each region, the cross section length is listed at the top-right in km, and in degrees at the bottom-right. Note that there are some imaging artifacts, for example, the dipping structures south of the slab depicted in cross sections B–D, that look like slabs. On the other hand, the flat lying slab on the 660 km discontinuity in cross sections P–R seems to be a real feature (see also Widiyantoro & van der Hilst 1997).

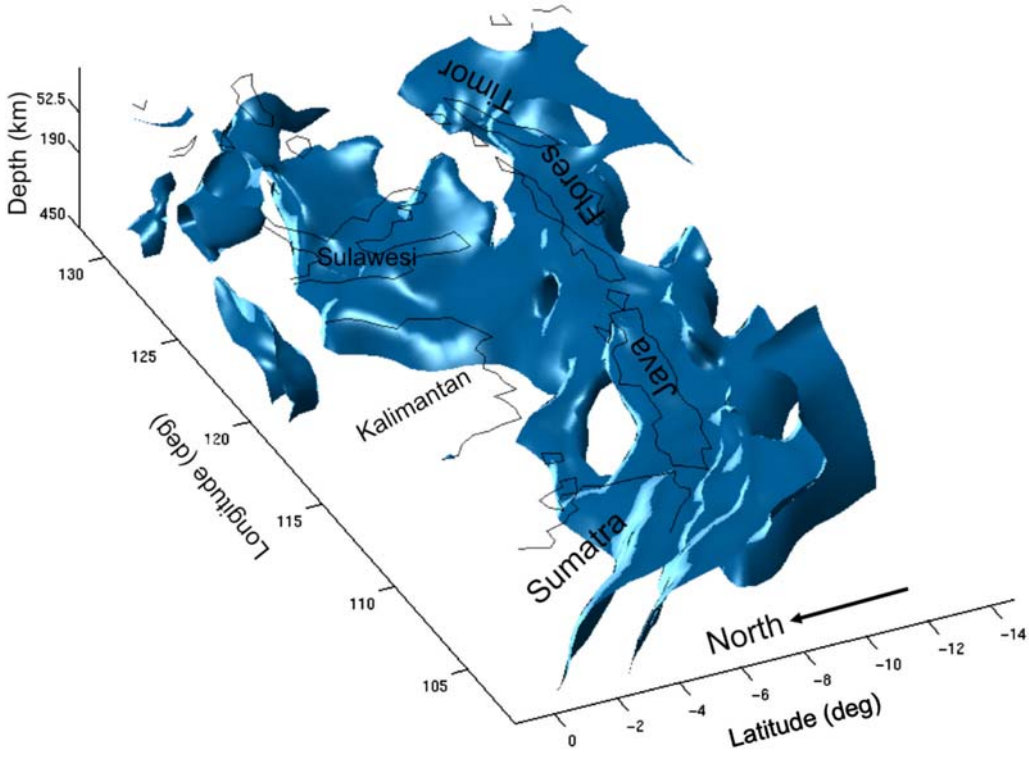

Fig. 5. Three-dimensional smoothed iso-surface plots for +0.85% P velocity perturbation relative to ak135 illustrating the subducted slab in the upper mantle beneath the eastern Sunda arc and the western part of the Banda arc viewed from the NW.

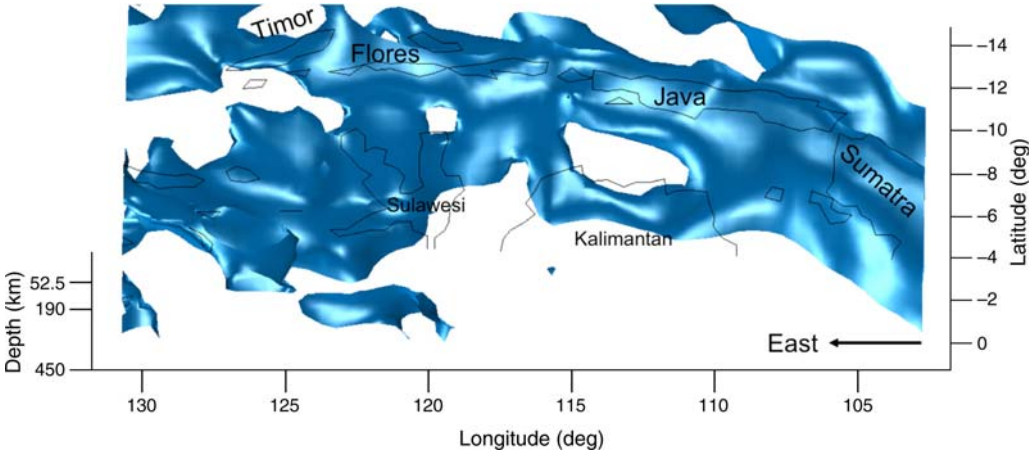

Fig. 6. Same as Figure 5, but viewed from the north. Notice the existence of a hole in the subducted slab below eastern Java, a tear in the slab beneath the easternmost part of the Sunda arc, and the small hole below Flores interpreted as a 'necking' of the slab.

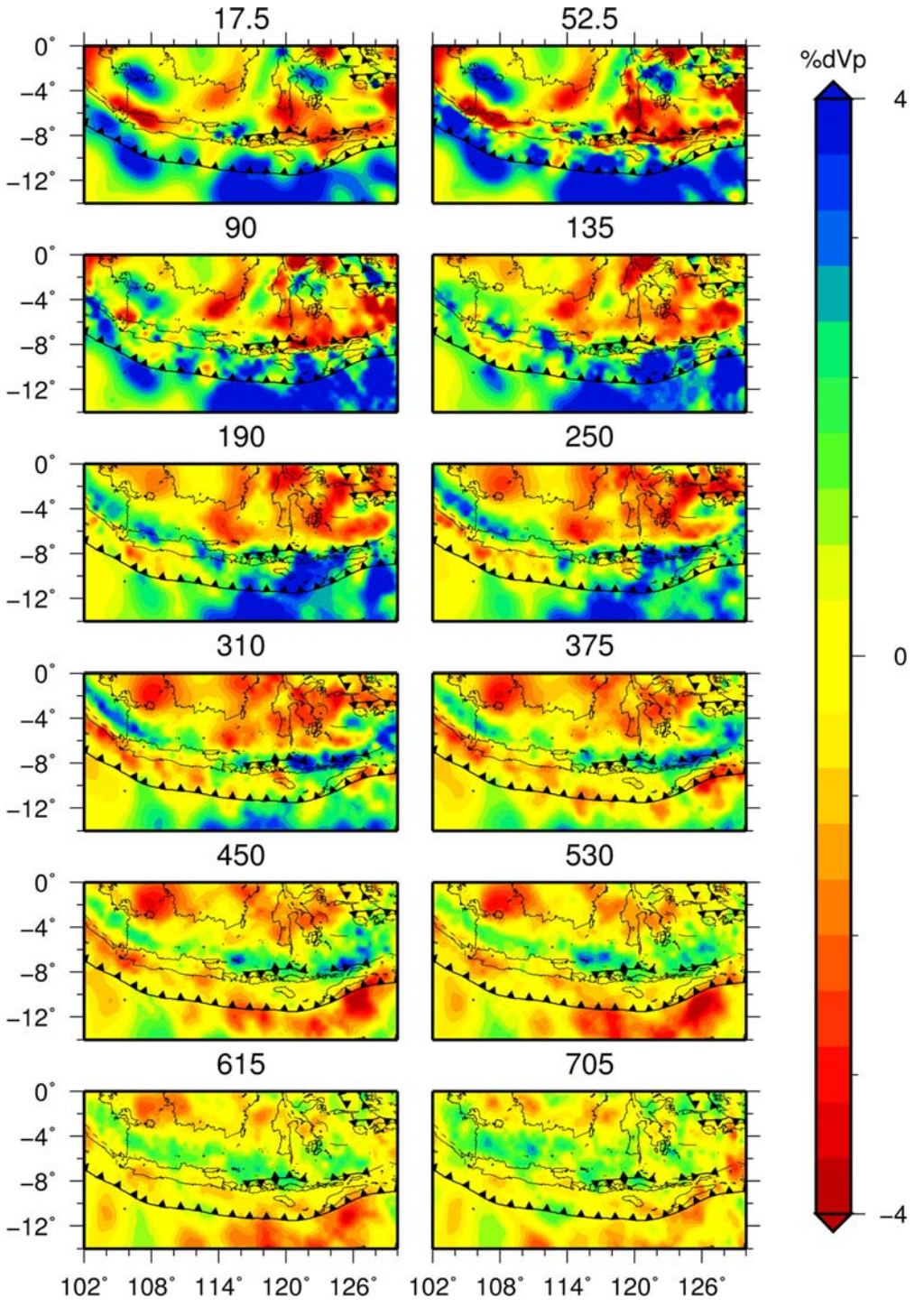

Fig. 7. Same as Figure 2, but derived using S-wave data and displayed using a 4% perturbation scale. Notice that the slab in the upper mantle parallel to the present-day trench is well imaged.

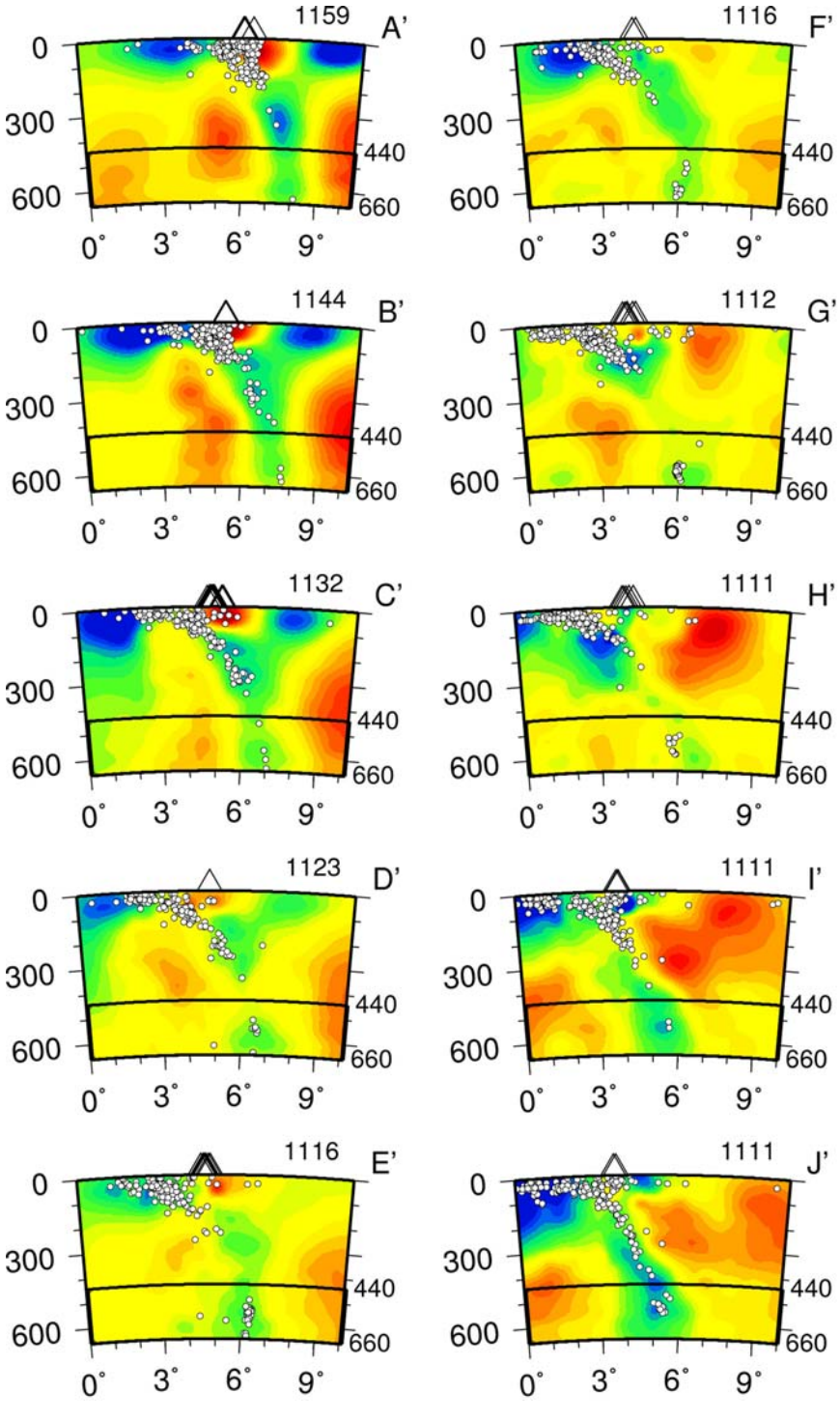

Fig. 8. Same as Figure 4, but derived using S-wave data and displayed using a 4% perturbation scale. Notice that the subducted slab is reasonably well imaged. However, the shallow structural feature beneath the back-arc region is less resolved due to lack of ray sampling.

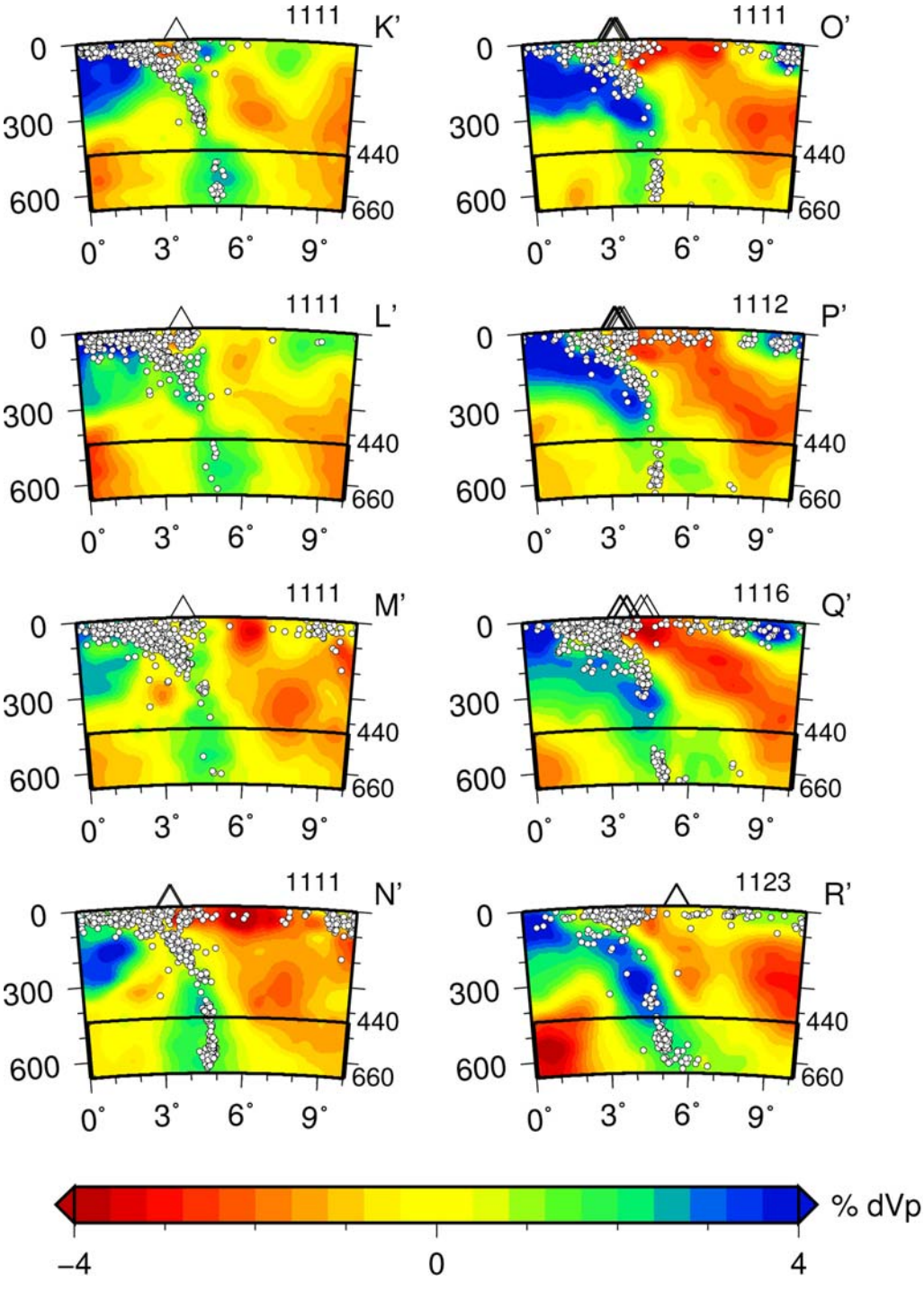

Fig. 8. *Continued.*

Discussion

Based on the results of our resolution tests (Fig. 3), the tear in the slab beneath eastern Java as depicted by the tomographic images (Figs 2–6) is judged to be a real feature. The tear is also observed in the high resolution P-wave tomographic model of Bijwaard & Spakman (2000). A number of processes could induce a tear in the down-going slab involving both crustal buoyancy variations and mantle processes acting on the slab. For example, Hall *et al.* (2009) suggested that the tear beneath eastern Java forms a hole in the subducted slab. This is related to the trench stepping back to the south after the slab broke due to the arrival of a buoyant plateau at *c*. 8 Ma that was unable to subduct. The convergence initially caused contractional deformation before the slab broke in front of the plateau. After the trench stepped back, subduction resumed behind the plateau causing the hole to develop (Hall *et al.* 2009). Similarly, a hole in the subducted slab has also been observed below the Izu–Bonin–Mariana trench by Miller *et al.* (2006). Miller *et al.* (2004, 2005) proposed that the Ogasawara Plateau collision and subsequent subduction are related to distortion and heterogeneity in the Pacific plate at depth. Using their new reconstruction of the subducted Pacific plate with a 3D visual model, Miller *et al.* (2006) inferred that the initiation of the oceanic plateau subduction at *c*. 8 Ma and the resulting complex slab morphology are related. For the Java case we agree with and support the interpretation by Hall *et al.* (2009). In addition, we note that any other process that either slows the rate of input into the trench relative to the rate of subduction of the slab within the Benioff zone or causes a trench jump would open a gap in the slab.

The tear in the slab beneath the easternmost part of the Sunda arc may be explained in a similar way. When Timor, part of the Australian continental plate, together with small islands to the east of it arrived at the former trench and collided with the Banda arc at *c*. 3 Ma (Hall 2002), it could not be subducted due to its high buoyancy. As a result, contractional deformation developed in the convergence zone and the slab broke, followed by the stepping back of the trench southward, forming the present-day Timor trough (B. Sapiie, pers. comm. 2009). This may have created the tear at shallow depth in the slab as the buoyant plateau arrived at 3 Ma. Presently, the region above the tear is marked by an aseismic zone around east Timor centred at 126°E and −9°S (see the seismicity plot in Fig. 1). In addition, the observed small hole in the subducted slab below Flores is interpreted as a thinning in or 'necking' of the slab, which may be related to the maximum tensional stress perpendicular to the trench in the region (Cloetingh & Wortel 1986).

In order to enhance our discussion, we compare the P-wave images with the S-wave ones. In spite of relatively noisy data, the results of the S data inversion are qualitatively in good agreement with those from the P data. The slab in the upper mantle is well imaged by the S data (Figs 7 & 8). One prominent difference is the absence of the deflected slab in the mantle transition zone below the eastern Sunda arc in the S images (cf. layer anomaly maps in Figs 2 & 7 at depths of around 530–615 km, and cross sections O–R in Figs 4 & 8). Such a difference was reported from regional seismic tomography of the NW Pacific island arcs using P- and S-wave arrival time data with similar ray path coverage (Widiyantoro *et al.* 1999). This implies that the stagnant lithospheric slab in the transition zone is more likely a bulk-sound structure, which is strongly supported by the results from joint inversions for bulk-sound and shear wavespeed (Kennett *et al.* 1998; Gorbatov & Kennett, 2003). For the Izu Bonin region, where trench migration has been reported, the properties of the deflected slab lying on top of the 660 km discontinuity show strong bulk-sound and weak shear signatures in contrast to the descending slab itself. A similar feature has also been observed below the Aegean region (Widiyantoro *et al.* 2004), where the slab is intensely distorted in the transition zone, with lower mantle penetration spatially confined to a relatively small area. The joint P- and S-inversion results also indicate that the deformed part of the slab is likely to be a bulk sound feature (Kennett *et al.* 1998). The difference between the shear and bulk sound signature of slabs that either deflect in the transition zone or penetrate to larger depths thus seems robust and may contain important information about the interaction of down wellings with the upper mantle discontinuities. The deflection of the slab in the transition zone below the eastern Sunda arc and the western Banda arc may resemble that observed beneath the Izu Bonin arc, the Aegean Sea as well as the Tyrrhenian Sea (Spakman *et al.* 1993), and can be related to the slab roll-back that has accompanied back-arc extension.

Because the P-wave data sampling is much denser than the S-wave sampling, one may wonder if the differences in the P- and S-wave images are due to differences in data coverage. To answer this question we have conducted additional P-wave tomographic imaging using similar ray path coverage as the S-wave data for the Indonesian region, as conducted for the NW Pacific island arcs by Widiyantoro *et al.* (1999). In general, the results depict structural features similar to those from the P-wave inversion results using full data coverage given in Figures 2–6. An example of vertical

sections across Bali through the P- and S-wave models derived using the common data coverage is given in Figure 9a, b. The P- and S-wave images depict not only the subducted Indo-Australian plate below Bali, but intriguingly also the south-dipping feature of the back-arc lithosphere directly north of Bali. The hypocentres of local earthquakes recorded by the Meteorological, Climatological and Geophysical Agency (MCGA) of Indonesia seismographic stations also form an image of southward dipping lithosphere underlying the Java Sea north of Bali (Widiyantoro & Fauzi 2005). Fault plane solutions of events at depths less than 50 km north of Bali in the period 1963–2001 compiled from several catalogues (mainly the Harvard Centroid Moment Tensor solution catalog; Global CMT Catalog 2009) generally depict thrust events (Figure 9c). We envisage that the southward dipping lithosphere underlying the Java Sea to the north of Bali may represent a south-dipping thrust due to back-arc shortening similar to that to the east (Flores).

The back-arc thrust of Flores generated a large tsunamigenic earthquake in 1992. In 2004, a devastating earthquake and subsequent strong tsunami occurred in Alor to the east of Timor. This event also occurred on a back-arc thrust that may represent the eastward extension of the Flores back-arc thrust fault. The tsunami catalogue of Indonesia shows that tsunamigenic earthquakes occurred in the area to the north and NE of Bali in 1816 and 1979, respectively (Hamzah *et al.* 2000). We interpret these events to be related to the south-dipping lithosphere in the back-arc region of Bali as revealed by the seismic tomograms (Fig. 9a, b).

Concluding remarks

We have presented seismic tomographic models of the 3D upper mantle velocity structure of the eastern Sunda arc from improved methods and data. The new images provide a more detailed structure of the subducted slab partly evident from the seismicity and enrich our understanding of the lithospheric processes governing its geodynamical evolution. The subducted slab seems to be continuous in the upper mantle along most of the eastern Sunda arc with some exceptions: (i) a hole in the slab in the mid upper mantle below eastern Java, and (ii) a tear in the slab in the uppermost mantle below Timor and small islands east of it. These observations may be related to the arrival of a buoyant plateau near eastern Java at *c*. 8 Ma and the arc–continent collision around Timor at *c*. 3 Ma, respectively. In addition, we also observed a 'necking' in the subducted slab below Flores.

The observed southward dipping feature below Bali is intriguing. This feature is in excellent

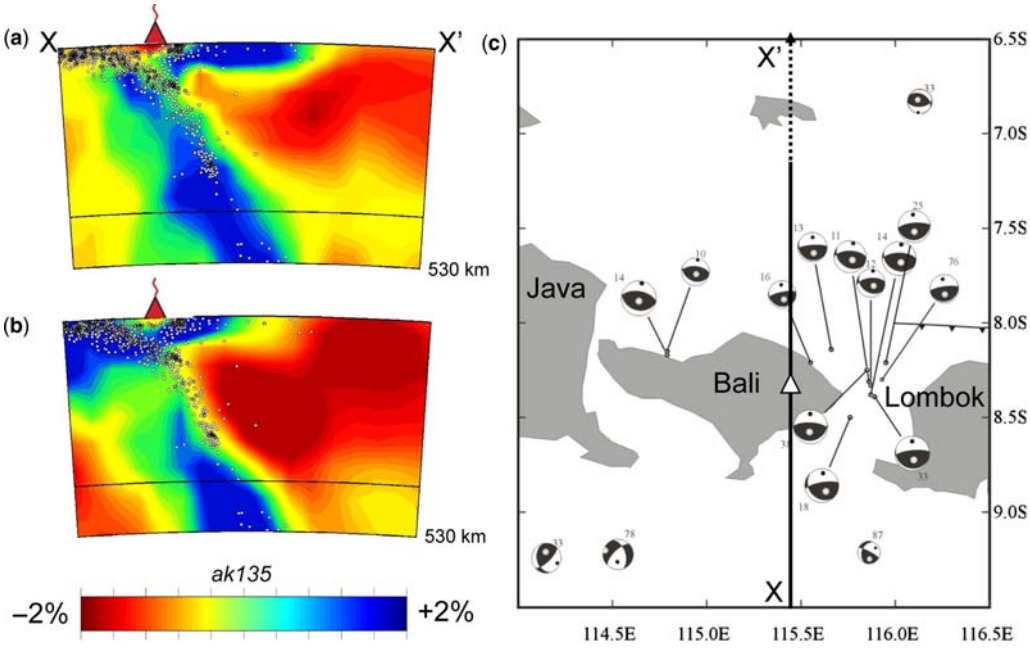

Fig. 9. (**a**) and (**b**) P- and S-wave tomograms respectively derived using similar ray path coverage, and (**c**) CMT solutions of shallow events in the back-arc region of Bali, courtesy of Fauzi, MCGA.

agreement with local seismicity and is also depicted clearly by P- and S-wave images derived using similar ray path coverage (Fig. 9), although some degree of smearing may exist due to the smoothing applied in the inversion.

The intriguing south-dipping feature in the back-arc region to the north of Bali has caused some tsunamigenic events. Following the great Andaman–Sumatran earthquake of 26 December 2004 with its attendant devastating tsunami, there have been calls for a tsunami early warning system for the Indian Ocean. Inferences from this study also urgently call for such an early warning system to mitigate tsunami hazards not only in the fore-arc, but also in the back-arc regions of Bali and small islands to the east.

The deflected slab below the easternmost part of the Sunda arc and most likely also below the Banda arc indicates that these regions have undergone slab roll-back. The deflected slab is clearly imaged in the P-wave model, but not in the S-wave model. This supports previous observations that the deflected slab in the mantle transition zone is likely a bulk-sound feature. Besides the excellent similarities depicted by the P- and S-wave images, the differences between the two models need to be investigated further. In order to explore the bulk and shear moduli, which have differing sensitivity to temperature and mineral composition, we need comparable high-resolution images of both P and S velocity distributions from high quality P-wave and S-wave data. They may then help to constrain the nature of processes that produce the observed variations. The next generation of subduction zone S-wave tomographic models would need more precise S-wave arrival times, such as those carefully processed by Grand (1994) for global tomography.

We thank E. R. Engdahl, R. D. van der Hilst and R. Buland for the updated hypocentre and phase data set used in this study, and Fauzi for fruitful discussion especially on the seismicity around the Bali region. Thanks also go to J. Granath and W. Spakman for helpful reviews, and R. Hall for useful comments. This material is based upon work supported in part by NASA, under award NNX06AF10G. S. W. would like to thank the ITB alumni association for a Fellowship (2009/2010) to conduct research on the structure of subduction zone and tectonics of the eastern Sunda arc.

References

Bassin, C., Laske, G. & Masters, G. 2000. The current limits of resolution for surface wave tomography in North America. *Eos, Transactions, American Geophysical Union*, **81**, F897.

Bijwaard, H. & Spakman, W. 2000. Non-linear global P-wave tomography by iterated linearized inversion. *Geophysical Journal International*, **141**, 71–82.

Bijwaard, H., Spakman, W. & Engdahl, E. R. 1998. Closing the gap between regional and global traveltime tomography. *Journal of Geophysical Research*, **103**, 30 055–30 078.

Cloetingh, S. A. P. L. & Wortel, M. J. R. 1986. Stress in the Indo-Australian plate. *Tectonophysics*, **132**, 49–67.

DeMets, C., Gordon, R. G., Argus, D. F. & Stein, S. 1994. Effect of recent revisions to the geomagnetic reversal time scale on estimates of current plate motions. *Geophysical Research Letters*, **21**, 2191–2194.

Engdahl, E. R., van der Hilst, R. D. & Buland, R. 1998. Global teleseismic earthquake relocation with improved travel times and procedures for depth determination. *Bulletin of the Seismological Society of America*, **88**, 722–743.

Engdahl, E. R., Villasenor, A., DeShon, H. R. & Thurber, C. H. 2007. Teleseismic relocation and assessment of seismicity (1918–2005) in the region of the 2004 Mw 9.0 Sumatra-Andaman and 2005 Mw 8.6 Nias Island great earthquakes. *Bulletin of the Seismological Society of America*, **97**, S43–61.

Fukao, Y., Obayashi, M., Inoue, H. & Nenbai, M. 1992. Subducting slabs stagnant in the mantle transition zone. *Journal of Geophysical Research*, **97**, 4809–4822.

GLOBAL CMT CATALOG 2009. *Global CMT web page*. http://www.globalcmt.org.

Gorbatov, A. & Kennett, B. L. N. 2003. Joint bulk-sound and shear tomography for western Pacific subduction zones. *Earth and Planetary Science Letters*, **210**, 527–543.

Grand, S. P. 1994. Mantle shear structure beneath the Americas and surrounding oceans. *Journal of Geophysical Research*, **99**, 11 591–11 621.

Hall, R. 2002. Cenozoic geological and plate tectonic evolution of SE Asia and the SW Pacific: computer-based reconstructions, model and animations. *Journal of Asian Earth Sciences*, **20**, 353–431.

Hall, R., Cross, L., Clements, B. & Spakman, W. 2009. Neogene subduction beneath Java: slab tearing, arc deformation and arc magmatism, and their causes. *In*: *Southeast Asian Gateway Evolution Conference (abstract)*. Royal Holloway University of London, United Kingdom.

Hamzah, L., Puspito, N. T. & Imamura, F. 2000. Tsumani catalog and zones in Indonesia. *Journal of Natural Disaster Sciences*, **22**, 25–43.

Kennett, B. L. N., Engdahl, E. R. & Buland, R. 1995. Constraints on seismic velocities in the Earth from traveltimes. *Geophysical Journal International*, **122**, 108–124.

Kennett, B. L. N., Widiyantoro, S. & van der Hilst, R. D. 1998. Joint seismic tomography for bulk-sound and shear wavespeed in the Earth's mantle. *Journal of Geophysical Research*, **103**, 12 469–12 493.

Koketsu, K. & Sekine, S. 1998. Pseudo-bending method for three-dimensional seismic ray tracing in a spherical earth with discontinuities. *Geophysical Journal International*, **132**, 339–346.

Miller, M. S., Kennett, B. L. N. & Lister, G. S. 2004. Imaging changes in morphology, geometry, and physical properties of the subducting Pacific plate along the Izu–Bonin–Mariana Arc. *Earth and Planetary Science Letters*, **224**, 363–370.

MILLER, M. S., GORBATOV, A. & KENNETT, B. L. N. 2005. Heterogeneity within the subducting Pacific slab beneath the Izu–Bonin–Mariana arc: evidence from tomography using 3-D ray-tracing inversion techniques. *Earth and Planetary Science Letters*, **235**, 331–342.

MILLER, M. S., KENNETT, B. L. N. & TOY, V. G. 2006. Spatial and temporal evolution of the subducting Pacific plate structure along the western Pacific margin. *Journal of Geophysical Research*, **111**, B02401, doi: 10.1029/2005JB003705.

MINSTER, J. B. & JORDAN, T. H. 1978. Present-day plate motions. *Journal of Geophysical Research*, **83**, 5331–5354.

MUELLER, R. D., ROEST, W. R., ROYER, J.-Y., GAHAGAN, L. M. & SCLATER, J. G. 1997. Digital isochrons of the world's ocean floor. *Journal of Geophysical Research*, **102**, 3211–3214.

NEWCOMB, K. R. & MCCANN, W. R. 1987. Seismic history and seismotectonics of the Sunda arc region. *Journal of Geophysical Research*, **92**, 421–439.

NOLET, G. 1987. Seismic wave propagation and seismic tomography. *In*: NOLET, G. (ed.) *Seismic Tomography*. Reidel, Dordrecht, Netherlands, 1–23.

PAIGE, C. & SAUNDERS, M. A. 1982. LSQR: an algorithm for sparse linear equations and least squares problems. *ACM Transaction on Mathematical Software*, **8**, 195–209.

PESICEK, J. D., THURBER, C. H., WIDIYANTORO, S., ENGDAHL, E. R. & DESHON, H. R. 2008. Complex slab subduction beneath northern Sumatra. *Geophysical Research Letters*, **35**, L20303, doi: 10.1029/2008GL035262.

PESICEK, J. D., THURBER, C. H., WIDIYANTORO, S., ENGDAHL, E. R., DESHON, H. R. & ZHANG, H. 2010. Sharpening the tomographic image of the subducting slab below Sumatra, the Andaman Islands, and Burma. *Geophysical Journal International*, **182**, 433–453.

PUSPITO, N. T., YAMANAKA, Y., MIYATAKE, T., SHIMAZAKI, K. & HIRAHARA, K. 1993. Three-dimensional P-wave velocity structure beneath the Indonesian region. *Tectonophysics*, **220**, 175–192.

SPAKMAN, W. & NOLET, G. 1988. Imaging algorithms, accuracy and resolution in delay time tomography. *In*: VLAAR, N. J., NOLET, G., WORTEL, M. J. R. & CLOETINGH, S. A. P. L. (eds) *Mathematical Geophysics; a Survey of Recent Developments in Seismology and Geodynamics*. Reidel, Dordrecht, Netherlands, 155–188.

SPAKMAN, W., VAN DER LEE, S. & VAN DER HILST, R. D. 1993. Travel-time tomography of the European-Mediterranean mantle down to 1400 km. *Physics of Earth Planetary Interiors*, **79**, 3–74.

TREGONING, P., BRUNNER, F. K. *ET AL*. 1994. First geodetic measurement of convergence across the Java Trench. *Geophysical Research Letters*, **21**, 2135–2138.

UM, J. & THURBER, C. H. 1987. A fast algorithm for two-point seismic ray tracing. *Bulletin of the Seismological Society of America*, **77**, 972–986.

WIDIYANTORO, S. & FAUZI 2005. Note on seismicity of the Bali convergent region in the eastern Sunda Arc, Indonesia. *Australian Journal of Earth Sciences*, **52**, 379–383.

WIDIYANTORO, S. & VAN DER HILST, R. D. 1996. Structure and evolution of lithospheric slab beneath the Sunda Arc, Indonesia. *Science*, **271**, 1566–1570.

WIDIYANTORO, S. & VAN DER HILST, R. D. 1997. Mantle structure beneath Indonesia inferred from high-resolution tomographic imaging. *Geophysical Journal International*, **130**, 167–182.

WIDIYANTORO, S., KENNETT, B. L. N. & VAN DER HILST, R. D. 1999. Seismic tomography with P and S data reveals lateral variations in the rigidity of deep slabs. *Earth and Planetary Science Letters*, **173**, 91–100.

WIDIYANTORO, S., GORBATOV, A., KENNETT, B. L. N. & FUKAO, Y. 2000. Improving global shear wave travel-time tomography using three-dimensional ray tracing and iterative inversion. *Geophysical Journal International*, **141**, 747–758.

WIDIYANTORO, S., VAN DER HILST, R. D. & WENZEL, F. 2004. Deformation of the Aegean slab in the mantle transition zone. *International Journal of Tomography and Statistics*, **D04**, 1–14.

ZHOU, H. & CLAYTON, R. W. 1990. P and S wave travel time inversions for subducting slabs under the island arcs of the northwest Pacific. *Journal of Geophysical Research*, **95**, 6829–6851.